HHS Public Access

Author manuscript

ACS Macro Lett. Author manuscript; available in PMC 2022 June 28.

Published in final edited form as:

ACS Macro Lett. 2021 December 21; 10(12): 1540–1548. doi:10.1021/acsmacrolett.1c00638.

DNA Conformation Dictates Strength and Flocculation in DNA–Microtubule Composites

Karthik R. Peddireddy,
Department of Physics and Biophysics, University of San Diego, San Diego, California 92110, United States

Davide Michieletto,
School of Physics and Astronomy, University of Edinburgh, Edinburgh EH9 3FD, United Kingdom; MRC Human Genetics Unit, Institute of Genetics and Molecular Medicine University of Edinburgh, Edinburgh EH4 2XU, United Kingdom

Gina Aguirre,
Department of Physics and Biophysics, University of San Diego, San Diego, California 92110, United States

Jonathan Garamella,
Department of Physics and Biophysics, University of San Diego, San Diego, California 92110, United States

Pawan Khanal,
Department of Physics and Biophysics, University of San Diego, San Diego, California 92110, United States

Rae M. Robertson-Anderson
Department of Physics and Biophysics, University of San Diego, San Diego, California 92110, United States

Abstract

Polymer topology has been shown to play a key role in tuning the dynamics of complex fluids and gels. At the same time, polymer composites, ubiquitous in everyday life, have been shown to exhibit emergent desirable mechanical properties not attainable in single-species systems. Yet, how topology impacts the dynamics and structure of polymer composites remains poorly

Corresponding Author Rae M. Robertson-Anderson randerson@sandiego.edu.

Notes

The authors declare no competing financial interest.

■ ASSOCIATED CONTENT

■ Supporting Information

The Supporting Information is available free of charge at https://pubs.acs.org/doi/10.1021/acsmacrolett.1c00638.

Section 1: Expanded Experimental Section; Figure S1: Measured forces in response to strain of rate $\dot{\gamma} = 9.4\ s^{-1}$ for DNA-MT composites; Figure S2: Nonlinear force responses of DNA-MT composites for different strain rates; Figure S3: Nonlinear force relaxations of DNA-MT composites following strains of different rates; Figure S4: Average spatial image autocorrelation curves of DNA-MT composites; Section 2: Theory for phase behavior of a composite of stiff and flexible polymers; Figure S5: Results of scaled particle theory using the correlation blob size ζ rather than R_G as the principal DNA length scale σ (PDF)

Complete contact information is available at: https://pubs.acs.org/10.1021/acsmacrolett.1c00638

understood. Here, we create composites of rigid rods (microtubules) polymerized within entangled solutions of flexible linear and ring polymers (DNA) of equal length. We couple optical tweezers microrheology with confocal microscopy and scaled particle theory to show that composites with linear DNA exhibit a strongly nonmonotonic dependence of elasticity and stiffness on microtubule concentration due to depletion-driven polymerization and flocculation of microtubules. In contrast, composites containing ring DNA show a much more modest monotonic increase in elastic strength with microtubule concentration, which we demonstrate arises from the decreased conformational size and increased miscibility of rings.

Graphical Abstract

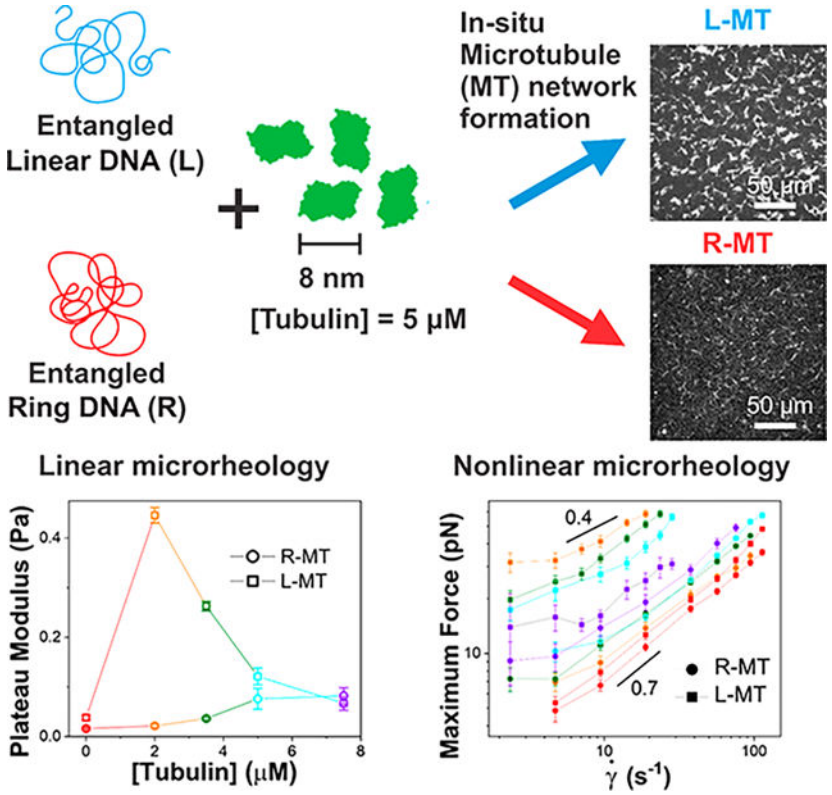

Polymer composites consisting of a polymer matrix reinforced with fillers[1–5] are of widespread importance in the natural and commercial world, with applications ranging from aerospace engineering to drug delivery.[6–12] Further, composites often exhibit emergent rheological and structural properties that are superior to those of the constituent materials.[2,4,5,13–20] For example, composites of stiff and flexible polymers can exhibit enhanced strength and stiffness while concomitantly reducing weight.[21–24] In cells, networks of stiff and semiflexible protein filaments (i.e., cytoskeleton) form in a dense solution of flexible and folded macromolecules such as nucleic acids and polysaccharides (i.e., cytoplasm). Mechanical interactions between the cytoplasm and cytoskeleton have been shown to be critical to the cell life cycle.[25–28] Finally, previous in vitro studies have shown that cytoskeletal composites exhibit emergent stress-stiffening and mechano-memory[13,29,30] due to entropically driven polymer rearrangement.

Despite the widespread interest and applicability of composites, the role of polymer end-closure in composite rheology remains largely unexplored.[31,32] At the same time, cyclization of linear polymers, which reduces the conformational size of coils, has been shown to play a primary role in the rheology of entangled polymers.[13,32–36] For example, linear polymers (with free ends) more effectively form entanglements and undergo affine deformation compared to ring polymers (with no free ends),[33,34] resulting in significantly enhanced elasticity and shear thinning. However, rings can become threaded by surrounding polymers, which can slow relaxation and increase viscoelasticity.[14,37–45] Further, ring-linear polymer blends have been shown to exhibit increased elasticity, stress-stiffening, and relaxation time scales compared to their single-topology counterparts.[14,32,46]

Here, we create composites of stiff microtubules and flexible linear and ring DNA molecules. We polymerize varying concentrations of tubulin into microtubules (MT) in the presence of entangled linear (L) and ring (R) DNA (at ~2.5X the critical entanglement concentration c_e)47 and determine the roles that DNA topology and tubulin concentration play in the microrheological properties and structure of DNA-MT composites (Figure 1). We show that DNA end-closure plays a prominent role in tubulin polymerization, network formation, and bundling, which ultimately dictates the mechanical response of the composites.

We first determine the dependence of the DNA conformation and tubulin concentration on linear elastic and viscous moduli, $G'(\omega)$ and $G''(\omega)$, which we extract from thermal oscillations of embedded trapped microspheres (Experimental Section, Figures 1 and 2). As shown in Figure 2a, the elastic modulus $G'(\omega)$ of R-MT composites increases monotonically with increasing tubulin concentrations over the entire frequency range, indicating increased elasticity. Further, at low tubulin concentrations, $G'(\omega)$ exhibits power-law scaling of ~0.3, which is reduced to ~0.1 for [tubulin] ≥ 5 μM, which is lower than the reported value of 0.17 for 10 μM MT solutions.48 The increased magnitude and decreased frequency-dependence of $G'(\omega)$ are both signatures of increased elasticity and connectivity, as one may expect given the increased density of stiff polymers.

In contrast to R-MTs, we observe a nonmonotonic dependence of $G'(\omega)$ on tubulin concentration in L-MT composites. As tubulin concentration increases from 0 to 2 μM, $G'(\omega)$ increases by an order of magnitude followed by a subsequent decrease as tubulin concentration increases to 7.5 μM. L-MTs also show reduced frequency-dependence of $G'(\omega)$ compared to linear DNA that is most apparent for the lowest tubulin concentration. Of note, despite this decrease in the L-MT elastic response at higher [tubulin], the R-MT elastic response remains lower and the frequency-dependence is stronger than L-MTs for all but the highest tubulin concentration (7.5 μM), likely due to the reduced ability of rings to form entanglements.[14,32] This topology dependence can also be seen in Figure 2d in which the approximate G^0 values, determined by evaluating G' at the frequency at which the loss tangent, $\tan\delta = G''/G'$, is a minimum,49 are plotted as a function of [tubulin]. Using reported G^0 values and scaling $G^0 \sim c^{1.4}$ for MT solutions, we estimate $G^0 \approx 0.05$ Pa for a 2 μM MT solution.48 In contrast, L-MTs with 2 μM tubulin exhibit an order of magnitude higher G^0 value, while R-MTs have a smaller value ($G^0 \approx 0.02$ Pa).

We also evaluate the complex viscosity, $\eta^*(\omega)$, as studies have shown that entangled ring and linear DNA both exhibit shear thinning $\eta^*(\omega) \sim \omega^{-a}$, but rings exhibit weaker thinning (smaller a) due to their reduced ability to align with flow.[14,3233,35] The addition of tubulin increases a to ~0.9 for both topologies, but R-MTs require 5 μM tubulin for this increase while 2 μM tubulin is sufficient for L-MTs. The delayed increase for R-MTs suggests that microtubule network formation may be more readily facilitated by linear DNA. At the same time, the apparent similarity in shear-thinning behavior for both composites suggests that microtubules may facilitate flow alignment of ring polymers to more readily allow for affine deformation, necessary for ample shear thinning.[34,50,51] Further, using data and scaling from ref 48, we estimate $\eta^*(\omega)$ values of ~0.2 to 0.009 Pa·s for 2 μM MT solutions over the frequency range we examine, an order of magnitude lower than what we find for L-MTs, and $a \approx 0.9$, similar to L-MT scaling but higher than that for R-MTs ($a \approx 0.65$).

To determine the robustness of the topology-dependent viscoelasticity to large strains, we measure the nonlinear force response (Figure 3). As shown, nonlinear stress curves for all composites initially rise steeply, with an elastic-like dependence, before reaching a more viscous regime with shallower force slopes. The addition of microtubules to both DNA types leads to an increase in force magnitude and slope at large distances, suggesting that composites are more readily able to retain elastic memory in the nonlinear regime compared to DNA solutions, which reach a nearly completely viscous response at the end of the strain. Further, the strong dependence of the force response on DNA end-closure and tubulin concentration seen in the linear regime is preserved. Namely, R-MTs exhibit a weak monotonic increase in force as a function of [tubulin] while L-MTs exhibit a strong nonmonotonic dependence. Further, at higher [tubulin], force curves exhibit peaks and valleys, which are more prevalent in L-MTs. We have seen similar “bumpiness” for actin-microtubule composites at high [tubulin] due to increased microscale heterogeneity.[52]

To quantify the strain-rate dependence, we evaluate the maximum force $F_{\max}$ reached during strain as a function of rate (Figure 3c). For reference, a fluid-like system should display a purely viscous response (i.e., $F_{\max} \sim \dot{\gamma}^1$), whereas a solid-like system should show minimal rate dependence ($F_{\max} \sim \dot{\gamma}^0$). As shown, all composites exhibit power-law dependence $F_{\max} \sim \dot{\gamma}^{\beta}$ for $\dot{\gamma} > 10\ s^{-1}$, with approximate exponents that depend on DNA topology and [tubulin]. Pure DNA solutions exhibit scaling $\beta \simeq 0.7$, independent of topology, in line with previous studies on ring-linear DNA blends14 and tube extension models for flexible polymers in the nonlinear regime.[53–55] While the addition of microtubules only modestly reduces the rate dependence for R-MTs ($\beta \geq 0.6$), the addition of 2 μM MTs to linear DNA reduces β to ~0.4. However, upon subsequent increase in [tubulin], β increases to ≥0.6. This result suggests that microtubules can synergistically interact more readily with linear DNA compared to rings to oppose flow-induced disentanglement. However, these interactions are most efficient at lower [tubulin].

Following strain, we measure the stress relaxation (Figure 4). While both DNA solutions relax nearly all of their stress during the measurement, all composites retain a nonzero residual force, indicative of elastic memory. Similar to previous studies on an entangled ring and linear DNA,14 we fit each relaxation curve to a sum of three exponential decays,

$F(t) = F_\infty + C_1 e^{-t/\tau_1} + C_2 e^{-t/\tau_2} + C_3 e^{-t/\tau_3}$, but here we include a nonzero residual force term F_∞. These fits yield three well-separated time constants (τ_1, τ_2, τ_3; Figure 4c) and residual forces that depend on [tubulin] and DNA topology (Figure 4a, inset). All τ_i, and F_∞ values show minimal rate dependence, represented by the error bars (Figure 4a,c,d), while the fractional amplitudes $\phi_i = C_i/(C_1 + C_2 + C_3)$ are rate-dependent (Figure 4e,f).

F_∞ values display a strong dependence on [tubulin], with the largest residual force at the lowest [tubulin] in L-MTs, and with L-MTs exhibiting higher values than R-MTs. The [tubulin] dependence of the time constants (τ_i) is substantially weaker but statistically significant in some instances. To understand the mechanisms underlying each time constant we compare our measured constants for entangled linear DNA to the principle relaxation time scales predicted for entangled linear polymers:56 the entanglement time τ_e over which diffusing chain segments reach the edge of the tube, the disengagement time τ_d over which the polymer reptates out of its initial deformed tube, and the Rouse time τ_r over which elastic relaxation of the deformed polymer occurs. The predicted time scales for our linear DNA solution are $\tau_e \cong 0.1$, s, $\tau_R \cong 0.5$ s, and $\tau_D \cong 9$ s.[56] As shown (Figure 4c), τ_1, τ_2, and τ_3 for linear DNA are comparable but slightly smaller than τ_e, and τ_d, respectively, likely due to nonlinear straining.57 The fractional amplitudes (Figure 4d,e) further support this interpretation as we see a large drop in ϕ_3 as $\dot{\gamma}$ increases, while ϕ_1 and ϕ_2, corresponding to τ_e and τ_r increase. Faster rates more easily disrupt entanglements and thus reduce the propensity for reptation, thereby increasing the relative contributions from τ_e and τ_R.

Comparing composites, L-MTs show a nonmonotonic dependence of relaxation dynamics on [tubulin], with all time constants increasing >2X upon addition of 2 μM tubulin, followed by subsequent reduction, while τ values for R-MTs lack significant [tubulin] dependence. A steeper drop in ϕ_3 in L-MTs further suggests that they are richer in entanglements compared to R-MTs as forced disentanglement is rate-dependent. Further, while rates up to 113 s^{-1} are possible in R-MTs, the trap could not withstand rates >30 s^{-1} in L-MTs, indicating stronger entanglements and DNA-MT interactions.

To further elucidate our microrheology results, we examine confocal micrographs of composites with rhodamine-labeled microtubules (Figure 5). As shown, without DNA, tubulin polymerizes into disconnected branched clusters that are heterogeneously distributed throughout the sample and grow and become more interconnected as [tubulin] increases.

Typically, crowding agents or depletants enhance polymerization reactions, including microtubule polymerization, due to entropically driven depletion effects.[58–63] Namely, the crowders aim to maximize their entropy by driving the polymerizing monomers together to reduce the excluded volume that surrounds each monomer. Surprisingly, we see an opposite effect in R-MTs: ring DNA hinders tubulin polymerization. A percolated microtubule network only emerges for [tubulin] ≥ 5, μM, consistent with our microrheology results (Figure 2) that show a discrete shift in $G'(\omega)$ scaling at 5, μM. We further note that the networks that form are more homogeneously distributed, with fewer clusters and branches compared to MTs alone, indicating that the entropic gain from mixing outweighs depletion interactions. Indeed, previous studies have shown that end-closure of polymers can significantly increase the miscibility of polymer blends.[64,65] This phenomenon may

be due to the smaller radius of gyration R_g of rings compared to linear chains of equal length ($R_{G,L} \simeq 1.58 R_{G,R}$),[66] which reduces the volume fraction taken up by the polymers (i.e., DNA), thereby lowering the depletion force that drives the other species (i.e., tubulin) to self-associate.[63,67] Another potential contribution is threading of rings by microtubules, which would aid mixing and further reduce the volume taken up by the rings (as some polymers are threaded by microtubules and no longer excluding their available volume), thus, reducing the depletion interaction strength. Previous studies have reported threading of ring DNA by cytoskeletal filaments,68 suggesting that rings, with diameter $\sigma_R \simeq 2R_{G,R} \simeq 1.04$ μm may indeed be threaded by microtubules ($D \simeq 25$ nm).

Opposite to R-MTs, L-MTs show a percolated MT network at 2, μM tubulin that is significantly more connected and pervasive than for MTs alone. This enhanced network formation, likely driven by depletion interactions,[69–71] explains the corresponding large increase in the force response. A percolated microtubule network provides a scaffold to reinforce the entangled DNA, while at the same time, entanglements with the linear DNA provide elastic support to the microtubules. As [tubulin] increases more microtubule bundling occurs, evidenced by brighter clusters with larger voids, which lowers the network connectivity, thereby weakening the microtubule scaffold, resulting in a drop in force response at higher [tubulin].

To quantify DNA-MT composite structure, we compute the spatial image autocorrelation $g(r)$ (Figure 5b). All $g(r)$ curves exhibit exponential rather than power-law decay suggestive of microphase separation instead of fractal structure.42 By fitting each curve to $g(r) \propto e^{r/\xi}$, we extract a characteristic correlation length ξ that describes the network structure. As shown, both DNA topologies decrease the correlation length of the MT network. R-MTs have the smallest ξ values for [tubulin]>2, μM, indicating that at any given [tubulin], microtubules are smaller than in the other cases, and, when a connected network forms, the mesh size is smaller as it is comprised of individual filaments rather than bundles or clusters. ξ values for L-MTs are significantly higher than for R-MTs and increase from 2 to 5, μM. As fully connected networks are evident at all [tubulin], this increase in ξ represents an increase in mesh size as microtubules flocculate. This flocculation in turn weakens the MT network by reducing entanglements and connections with DNA, thus explaining the drop in force for [tubulin] > 2 μM.

To further explain our observations we use scaled particle theory (SPT)72 to compute the phase diagram of a solution of rod-like colloids (MTs) and flexible coils (DNA; Figure 6). Within this framework, described in the SI, DNA depletants induce an isotropic-to-nematic transition for MTs for certain values of DNA and MT volume fractions, as shown by the binodals in Figure 6. The region of phase space between the binodals represents the coexistence of isotropic and nematic MT phases. In both phases flanking the coexistence region, microtubules and DNA are mixed, while in the coexistence phase they are demixed and isotropic and nematic microtubule arrangements are present. In experiments, this is seen as flocs of nematically aligned microtubules that are isotropically distributed throughout the DNA network (Figure 5). While SPT predicts macroscopic phase separation of nematic and isotropic phases in the coexistence region, we instead observe microphase separation (flocculation), likely due to slow relaxation modes (evidenced by nonzero F_∞), and

interactions not accounted for in the model (e.g., entanglements, threadings). Intriguingly, DNA depletants significantly widen the coexistence region from that of a simple solution of rod rodlike colloids.[73,74]

To account for the different DNA topologies, we consider the topology-dependent conformational sizes σ (~$2R_G$) of ring and linear DNA of equal length (i.e., $\sigma_L \simeq 1.58\sigma_r$).66 SPT does not explicitly account for end-closure or topology otherwise, so the results for ring DNA are the same as for a ~ $2.2x$ (i.e., $(R_{g,l}/R_{G,R})^{1/0.58}$) 66 shorter linear polymer. Our calculations show that rings (i.e., smaller coils) are substantially less effective at inducing microtubule flocculation, as evidenced by the smaller coexistence regime and the higher MT concentrations required to reach isotropic–nematic coexistence. The smaller coexistence region further shows that the nematic MT phase is less dense in the presence of rings compared to linear DNA (Figure 6), implying that density modulation is weaker and therefore less likely to impact the mechanical properties of the R-MT composite.

As described in Figure 1, our ring DNA solution contains ~10% linear DNA (see the SI). The presence of linear contaminants likely leads to enhanced entanglement dynamics compared to a solution of pure rings.32 Linear contaminants may also shift the onset of tubulin polymerization and DNA-MT demixing to lower [tubulin]. While a small fraction of linear contaminants can have dramatic effects on the rheology of ring polymers, the effect is to bring the rheological properties closer in line with those of linear polymer solutions.38 As such, we expect that for a pure ring DNA solution, the topological effects on DNA-MT composites may be even more dramatic, but the trends and physical picture will remain the same. Similarly, threading of rings would amplify the topology-dependent effects in SPT as it would effectively lower the volume fraction of polymer coils. One can look to regions of the phase diagram (Figure 6) that have a lower DNA volume fraction to predict the phase behavior with threading present.

Previous works examining depletion interactions between colloids in polymer solutions have shown that, when polymers are highly overlapping, the principal length scale that dictates depletion interactions in some cases is the correlation blob size ζ of the polymers rather than R_G (or σ).[75,76] Similar to R_G, the blob size for ring DNA is smaller than that for linear DNA ($\zeta_L \cong 1.8\zeta_R$, see the SI), and the corresponding SPT phase diagram is qualitatively the same (Figure S5).

Finally, we point out that initially, tubulin, of higher molarity and smaller size than DNA may serve as the depletant, promoting demixing of the two species. This entropic force would be greater for linear DNA than for rings given the larger volume they take up in solution (~σ^3). As tubulin polymerizes and becomes larger than the DNA coils then the DNA becomes the depletant, driving tubulin polymerization and flocculation. Once again, depletion interactions in L-MTs will be stronger than for R-MTs due to their larger volume which increases the osmotic driving force (proportional to σ).

In conclusion, our optical tweezers microrheology and confocal microscopy studies on DNA-MT composites, combined with SPT calculations, show that subtle changes in polymer conformation (free or closed ends) can have dramatic effects on the structure and

mechanics of polymer composites. Linear DNA promotes microtubule network formation and flocculation while ring DNA of equal length (and thus smaller conformational size), hinders it, which leads to a substantially larger force response in L-MTs compared to R-MTs, as well as a unique nonmonotonic dependence of elastic strength on tubulin concentration. Our results shed important new light on the role that end-closure plays in the rheology and structure of polymer composites, which has broad reaching implications in biology, chemical engineering, and materials applications.

■ EXPERIMENTAL SECTION

Many of the materials and methods are described in the preceding sections and in the captions of Figures 1–6. More detailed descriptions of all experimental materials and methods as well as theoretical calculations are included in the Supporting Information.

Supplementary Material

Refer to Web version on PubMed Central for supplementary material.

ACKNOWLEDGMENTS

The authors acknowledge financial support from the Air Force Office of Scientific Research (AFOSR-FA9550-17-1-0249). The authors also acknowledge Prof. Jennifer L. Ross (Syracuse University) for useful discussions regarding microtubule preparation and handling.

■ REFERENCES

(1). Chawla KK Composite Materials: Science and Engineering; Springer Science & Business Media, 2012.

(2). Hsissou R; Seghiri R; Benzekri Z; Hilali M; Rafik M; Elharfi A Polymer composite materials: A comprehensive review. Composite Structures 2021, 262, 113640.

(3). Jose JP; Joseph K Advances in Polymer Composites: Macro- and Microcomposites – State of the Art, New Challenges, and Opportunities. Polymer Composites; Wiley, 2012; pp 1–16.

(4). Gupta RK Polymer and Composite Rheology; CRC Press, 2000.

(5). Larson RG The Structure and Rheology of Complex Fluids; Oxford University Press: New York, 1999; Vol. 150.

(6). Huang H-M Medical Application of Polymer-Based Composites. Polymers 2020, 12 (11), 2560.

(7). Friedrich K; Almajid AA Manufacturing Aspects of Advanced Polymer Composites for Automotive Applications. Appl. Compos. Mater. 2013, 20 (2), 107–128.

(8). Holbery J; Houston D Natural-fiber-reinforced polymer composites in automotive applications. JOM 2006, 58 (11), 80–86.

(9). Friedrich K; Chang L; Haupert F Current and future applications of polymer composites in the field of tribology. Composite Materials; Springer, 2011; pp 129–167.

(10). Krishnamurthy VN Polymers in Space Environments. In Polymers and Other Advanced Materials: Emerging Technologies and Business Opportunities; Prasad PN, Mark JE, Fai TJ, Eds.; Springer US: Boston, MA, 1995; pp 221–226.

(11). Irving PE; Soutis C Polymer Composites in the Aerospace Industry; Woodhead Publishing, 2019.

(12). Wei R; Hua X; Xiong Z Polymers and Polymeric Composites with Electronic Applications; Hindawi, 2018.

(13). Fitzpatrick R; Michieletto D; Peddireddy KR; Hauer C; Kyrillos C; Gurmessa BJ; Robertson-Anderson RM Synergistic Interactions Between DNA and Actin Trigger Emergent Viscoelastic Behavior. Phys. Rev. Lett. 2018, 121 (25), 257801. [PubMed: 30608839]

(14). Peddireddy KR; Lee M; Schroeder CM; Robertson-Anderson RM Viscoelastic properties of ring-linear DNA blends exhibit nonmonotonic dependence on blend composition. Physical Review Research 2020, 2 (2), 023213.

(15). Hsissou R; Elharfi A Rheological behavior of three polymers and their hybrid composites (TGEEBA/MDA/PN), (HGEMDA/MDA/PN) and (NGHPBAE/MDA/PN). J. King Saud Univ., Sci 2020, 32 (1), 235–244.

(16). Díez-Pascual A Synthesis and Applications of Biopolymer Composites. Int. J. Mol. Sci. 2019, 20, 2321.

(17). Jancar J; Douglas JF; Starr FW; Kumar SK; Cassagnau P; Lesser AJ; Sternstein SS; Buehler MJ Current issues in research on structure–property relationships in polymer nan-ocomposites. Polymer 2010, 51 (15), 3321–3343.

(18). Yu Z; Tantakitti F; Yu T; Palmer LC; Schatz GC; Stupp SI Simultaneous covalent and noncovalent hybrid polymerizations. Science 2016, 351 (6272), 497–502. [PubMed: 26823427]

(19). Niu R; Gong J; Xu D; Tang T; Sun Z-Y Influence of molecular weight of polymer matrix on the structure and rheological properties of graphene oxide/polydimethylsiloxane composites. Polymer 2014, 55 (21), 5445–5453.

(20). AlMaadeed MA; Ouederni M; Noorunnisa Khanam P Effect of chain structure on the properties of Glass fibre/polyethylene composites. Mater. Eng. 2013, 47, 725–730.

(21). Takayanagi M; Ogata T; Morikawa M; Kai T Polymer composites of rigid and flexible molecules: System of wholly aromatic and aliphatic polyamides. J. Macromol. Sci., Part B: Phys 1980, 17 (4), 591–615.

(22). Takayanagi M; Goto K Polymer composite of rigid and flexible molecules: Blend systems of poly(p-phenylene terephthalamide) and ABS resin. J. Appl. Polym. Sci. 1984, 29 (8), 2547–2559.

(23). Hamad K; Kaseem M; Ayyoob M; Joo J; Deri F Polylactic acid blends: The future of green, light and tough. Prog. Polym. Sci. 2018, 85, 83–127.

(24). Zadorecki P; Michell AJ Future prospects for wood cellulose as reinforcement in organic polymer composites. Polym. Compos. 1989, 10 (2), 69–77.

(25). Field CM; Wuhr M; Anderson GA; Kueh HY; Strickland D; Mitchison TJ Actin behavior in bulk cytoplasm is cell cycle regulated in early vertebrate embryos. J. Cell Sci. 2011, 124 (12), 2086. [PubMed: 21610091]

(26). Hohmann T; Dehghani F The Cytoskeleton—A Complex Interacting Meshwork. Cells 2019, 8 (4), 362.

(27). Hu J; Jafari S; Han Y; Grodzinsky AJ; Cai S; Guo M Size- and speed-dependent mechanical behavior in living mammalian cytoplasm. Proc. Natl. Acad. Sci. U. S. A. 2017, 114 (36), 9529. [PubMed: 28827333]

(28). Xie J; Minc N Cytoskeleton Force Exertion in Bulk Cytoplasm. Front. Cell Dev. Biol. 2020, 8 (69), na DOI: 10.3389/fcell.2020.00069.

(29). Farhadi L; Ricketts SN; Rust MJ; Das M; Robertson-Anderson RM; Ross JL Actin and microtubule crosslinkers tune mobility and control co-localization in a composite cytoskeletal network. Soft Matter 2020, 16 (31), 7191–7201. [PubMed: 32207504]

(30). Ricketts SN; Francis ML; Farhadi L; Rust MJ; Das M; Ross JL; Robertson-Anderson RM Varying crosslinking motifs drive the mesoscale mechanics of actin-microtubule composites. Sci. Rep. 2019, 9 (1), 12831. [PubMed: 31492892]

(31). Dealy JM; Read DJ; Larson RG. Structure and Rheology of Molten Polymers: From Structure to Flow Behavior and Back Again; Carl Hanser Verlag GmbH Co KG, 2018.

(32). Vlassopoulos D; Pasquino R; Snijkers F Progress in the Rheology of Cyclic Polymers. Topological Polymer Chemistry; World Scientific, 2012; pp 291–316.

(33). Parisi D; Costanzo S; Jeong Y; Ahn J; Chang T; Vlassopoulos D; Halverson JD; Kremer K; Ge T; Rubinstein M; Grest GS; Srinin W; Grosberg AY Nonlinear Shear Rheology of Entangled Polymer Rings. Macromolecules 2021, 54 (6), 2811–2827.

(34). Huang Q; Ahn J; Parisi D; Chang T; Hassager O; Panyukov S; Rubinstein M; Vlassopoulos D Unexpected Stretching of Entangled Ring Macromolecules. Phys. Rev. Lett. 2019, 122 (20), 208001. [PubMed: 31172770]

(35). Vlassopoulos D Macromolecular topology and rheology: beyond the tube model. Rheol. Acta 2016, 55 (8), 613–632.

(36). Yan Z-C; Costanzo S; Jeong Y; Chang T; Vlassopoulos D Linear and Nonlinear Shear Rheology of a Marginally Entangled Ring Polymer. Macromolecules 2016, 49 (4), 1444–1453.

(37). Subramanian G; Shanbhag S Conformational properties of blends of cyclic and linear polymer melts. Phys. Rev. E: Stat. Nonlin. Soft Matter Phys 2008, 77 (1), 011801. [PubMed: 18351867]

(38). Kapnistos M; Lang M; Vlassopoulos D; Pyckhout-Hintzen W; Richter D; Cho D; Chang T; Rubinstein M Unexpected power-law stress relaxation of entangled ring polymers. Nat. Mater. 2008, 7 (12), 997–1002. [PubMed: 18953345]

(39). Halverson JD; Grest GS; Grosberg AY; Kremer K Rheology of Ring Polymer Melts: From Linear Contaminants to Ring-Linear Blends. Phys. Rev. Lett. 2012, 108 (3), 038301. [PubMed: 22400790]

(40). Doi Y; Matsubara K; Ohta Y; Nakano T; Kawaguchi D; Takahashi Y; Takano A; Matsushita Y Melt Rheology of Ring Polystyrenes with Ultrahigh Purity. Macromolecules 2015, 48, 3140–3147, DOI: 10.1021/acs.macromol.5b00076.

(41). Richter D; Gooßen S; Wischnewski A Celebrating Soft Matter's 10th Anniversary: Topology matters: structure and dynamics of ring polymers. Soft Matter 2015, 11 (44), 8535–8549. [PubMed: 26406787]

(42). Abadi M; Serag MF; Habuchi S Single-Molecule Imaging Reveals Topology Dependent Mutual Relaxation of Polymer Chains. Macromolecules 2015, 48 (17), 6263–6271.

(43). Doi Y; Matsumoto A; Inoue T; Iwamoto T; Takano A; Matsushita Y; Takahashi Y; Watanabe H Re-examination of terminal relaxation behavior of high-molecular-weight ring polystyrene melts. Rheol. Acta 2017, 56 (6), 567–581.

(44). Parisi D; Ahn J; Chang T; Vlassopoulos D; Rubinstein M Stress Relaxation in Symmetric Ring-Linear Polymer Blends at Low Ring Fractions. Macromolecules 2020, 53 (5), 1685–1693. [PubMed: 33518807]

(45). Borger A; Wang W; O'Connor TC; Ge T; Grest GS; Jensen GV; Ahn J; Chang T; Hassager O; Mortensen K; Vlassopoulos D; Huang Q Threading–Unthreading Transition of Linear-Ring Polymer Blends in Extensional Flow. ACS Macro Lett. 2020, 9 (10), 1452–1457. [PubMed: 35653662]

(46). Chapman CD; Shanbhag S; Smith DE; Robertson-Anderson RM. Complex effects of molecular topology on diffusion in entangled biopolymer blends. Soft Matter 2012, 8 (35), 9177–9182.

(47). Robertson RM; Smith DE Self-Diffusion of Entangled Linear and Circular DNA Molecules:Dependence on Length and Concentration. Macromolecules 2007, 40 (9), 3373–3377.

(48). Lin Y-C; Koenderink GH; MacKintosh FC; Weitz DA Viscoelastic Properties of Microtubule Networks. Macromolecules 2007, 40 (21), 7714–7720.

(49). Liu C; He J; Ruymbeke E. v.; Keunings R; Bailly C Evaluation of different methods for the determination of the plateau modulus and the entanglement molecular weight. Polymer 2006, 47 (13), 4461–4479.

(50). Tu MQ; Lee M; Robertson-Anderson RM; Schroeder CM Direct Observation of Ring Polymer Dynamics in the Flow-Gradient Plane of Shear Flow. Macromolecules 2020, 53 (21), 9406–9419.

(51). Peddireddy KR; Lee M; Zhou Y; Adalbert S; Anderson S; Schroeder CM; Robertson-Anderson RM Unexpected entanglement dynamics in semidilute blends of supercoiled and ring DNA. Soft Matter 2020, 16 (1), 152–161. [PubMed: 31774103]

(52). Ricketts SN; Ross JL; Robertson-Anderson RM CoEntangled Actin-Microtubule Composites Exhibit Tunable Stiffness and Power-Law Stress Relaxation. Biophys. J. 2018, 115 (6), 1055–1067. [PubMed: 30177441]

(53). Teixeira RE; Dambal AK; Richter DH; Shaqfeh ESG; Chu S The Individualistic Dynamics of Entangled DNA in Solution. Macromolecules 2007, 40 (7), 2461–2476.

(54). Desai PS; Larson RG Constitutive model that shows extension thickening for entangled solutions and extension thinning for melts. J. Rheol. 2014, 58 (1), 255–279.

(55). Masubuchi Y Simulating the Flow of Entangled Polymers. Annu. Rev. Chem. Biomol Eng. 2014, 5 (1), 11–33. [PubMed: 24498953]

(56). Doi M; Edwards SF The Theory of Polymer Dynamics; Oxford University Press: New York, 1986; Vol. 73.

(57). Chapman CD; Robertson-Anderson RM Nonlinear Microrheology Reveals Entanglement-Driven Molecular-Level Viscoelasticity of Concentrated DNA. Phys. Rev. Lett. 2014, 113 (9), 098303. [PubMed: 25216012]

(58). Minton AP Excluded volume as a determinant of macromolecular structure and reactivity. Biopolymers 1981, 20 (10), 2093–2120.

(59). McGuffee SR; Elcock AH Diffusion, crowding & protein stability in a dynamic molecular model of the bacterial cytoplasm. PLoS Comput. Biol. 2010, 6 (3), No. e1000694. [PubMed: 20221255]

(60). Zhou H-X; Rivas G; Minton AP Macromolecular Crowding and Confinement: Biochemical, Biophysical, and Potential Physiological Consequences. Annu. Rev. Biophys. 2008, 37 (1), 375–397. [PubMed: 18573087]

(61). Wieczorek M; Chaaban S; Brouhard GJ Macromolecular Crowding Pushes Catalyzed Microtubule Growth to Near the Theoretical Limit. Cell. Mol. Bioeng. 2013, 6 (4), 383–392.

(62). Tseng H-C; Graves DJ Natural Methylamine Osmolytes, Trimethylamine N-Oxide and Betaine, Increase Tau-Induced Polymerization of Microtubules. Biochem. Biophys. Res. Commun. 1998, 250 (3), 726–730. [PubMed: 9784413]

(63). Schummel PH; Gao M; Winter R Modulation of the Polymerization Kinetics of α/β-Tubulin by Osmolytes and Macromolecular Crowding. ChemPhysChem 2017, 18 (2), 189–197. [PubMed: 27813294]

(64). Kobayashi Y; Doi Y; Abdul Rahman SS; Kim E; Kim TH; Takano A; Matsushita Y SANS Study of Ring Topology Effects on the Miscibility of Polymer Blends. Macromolecules 2018, 51 (5), 1885–1893.

(65). Sakaue T; Nakajima CH Miscibility phase diagram of ring-polymer blends: A topological effect. Phys. Rev. E: Stat. Phys., Plasmas, Fluids, Relat. Interdiscip. Top. 2016, 93 (4), 042502.

(66). Robertson RM; Laib S; Smith DE Diffusion of isolated DNA molecules: Dependence on length and topology. Proc. Natl. Acad. Sci. U. S. A. 2006, 103 (19), 7310–7314. [PubMed: 16648255]

(67). Mitchison TJ Colloid osmotic parameterization and measurement of subcellular crowding. Mol. Biol. Cell 2019, 30 (2), 173–180. [PubMed: 30640588]

(68). Garamella J; Regan K; Aguirre G; McGorty RJ; Robertson-Anderson RM Anomalous and heterogeneous DNA transport in biomimetic cytoskeleton networks. Soft Matter 2020, 16 (27), 6344–6353. [PubMed: 32555863]

(69). Asakura S; Oosawa F On interaction between two bodies immersed in a solution of macromolecules. J. Chem. Phys. 1954, 22 (7), 1255–1256.

(70). Gregory J; Barany S Adsorption and flocculation by polymers and polymer mixtures. Adv. Colloid Interface Sci. 2011, 169 (1), 1–12. [PubMed: 21762869]

(71). Vajihinejad V; Gumfekar SP; Bazoubandi B; Rostami Najafabadi Z; Soares JBP Water Soluble Polymer Flocculants: Synthesis, Characterization, and Performance Assessment. Macromol. Mater. Eng. 2019, 304 (2), 1800526.

(72). Lekkerkerker HNW; Stroobants A Phase behaviour of rodlike colloid+flexible polymer mixtures. Nuovo Cimento Soc. Ital. Fis., D 1994, 16 (8), 949.

(73). Warren PB Depletion effect in a model lyotropic liquid crystal-theory. J. Phys. I 1994, 4 (2), 237–244.

(74). Flory PJ Statistical Thermodynamics of Mixtures of Rodlike Particles. 5. Mixtures with Random Coils. Macromolecules 1978, 11 (6), 1138–1141.

(75). Verma R; Crocker JC; Lubensky TC; Yodh AG Entropic Colloidal Interactions in Concentrated DNA Solutions. Phys. Rev. Lett. 1998, 81 (18), 4004–4007.

(76). Verma R; Crocker JC; Lubensky TC; Yodh AG Attractions between Hard Colloidal Spheres in Semiflexible Polymer Solutions. Macromolecules 2000, 33 (1), 177–186.

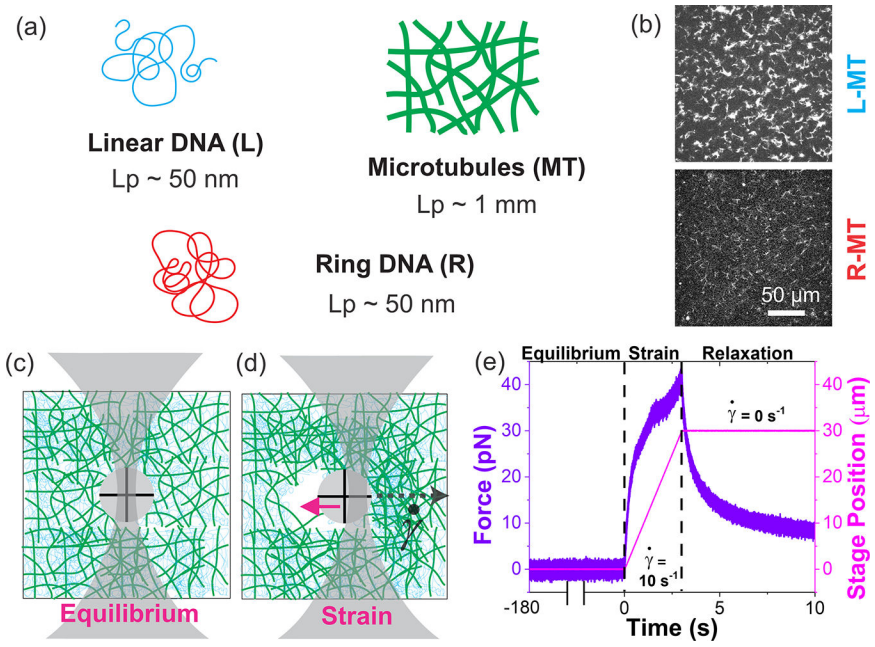

Figure 1.

Elucidating the microrheological properties of composites of rigid microtubules and flexible ring and linear DNA. (a) Cartoons of linear (L, blue) and ring (R, red) DNA of identical contour lengths (115 kbp, 39 μm) and microtubules (MT, green). (b) Confocal micrographs of composites of 5 μM rhodamine-labeled tubulin polymerized into microtubules in solutions of 0.65 mg/mL (~2.5c_e) linear (top, L-MT) and ring (bottom, R-MT) DNA (unlabeled). The nominal ring DNA solution and R-MT composites are composed of ~90% ring DNA and 10% linear DNA due to shearing of rings that occurs during the purification process (see SI). The scale bar applies to both micrographs. (c–e) Cartoons of linear (c) and nonlinear (d) optical tweezers microrheology. A microsphere of radius R = 2.25 μm (gray circle) embedded in a L-MT composite is trapped using a focused laser beam (gray). (e) Thermal oscillations of the bead in equilibrium are used to determine the linear viscoelastic moduli via the generalized Stokes–Einstein relation (see Experimental Section). To measure the nonlinear rheological response, the same optically trapped bead is displaced 30 μm (γ = 6.7) through DNA-MT composites at speeds $\left(\dot{\gamma} = 3v/\sqrt{2}R = 2.4 - 113\ \mathrm{s}^{-1}\right)$. Following strain, the composite is allowed to relax, and the microsphere returns to the trap center. Stage position (magenta) and force exerted on the trapped bead (violet) during equilibrium (180 s), strain (0.25–12 s), and relaxation (8–20 s) are recorded at 20 kHz. Data shown is for a u = 10 μm/s strain exerted on an L-MT composite with 2 μM tubulin.

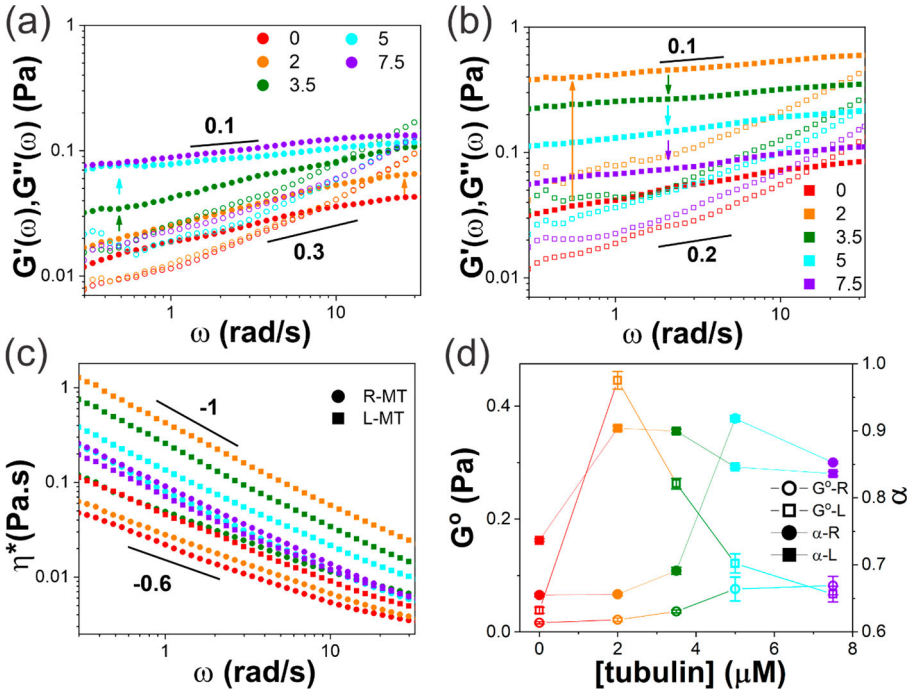

Figure 2.

Linear frequency-dependent viscoelastic moduli of DNA-MT composites exhibit strong dependence on DNA end-closure. (a, b) Frequency-dependent elastic and viscous moduli, $G'(\omega)$ (closed symbols) and $G''(\omega)$ (open symbols) for DNA-MT composites with ring (a, circles) and linear (b, squares) DNA and varying tubulin concentrations (listed in μM in legend). Arrows point in the direction of increasing tubulin concentration to guide the eye. $G'(\omega)$ curves exhibit a strong nonmonotonic dependence on tubulin concentration for linear DNA. (c) Complex viscosity $\eta^*(\omega)$ for R-MT (circles) and L-MT (squares) composites show shear-thinning $\eta^*(\omega) \sim \omega^{-\alpha}$ with exponents that depend on DNA topology. Black lines denote power-laws with exponents listed. (d) Elastic plateau modulus G^0 (open symbols) determined from the minimum in $\tan\delta = G''/G'$, and shear-thinning exponent α (closed symbols) determined from power-law fits to η^*(0.3 rad/s < ω <10 rad/s), plotted for R-MT (circles) and L-MT (squares) composites as a function of tubulin concentration ([tubulin]). Error bars, many of which are smaller than the symbol size, represent the standard error from 15 trials.

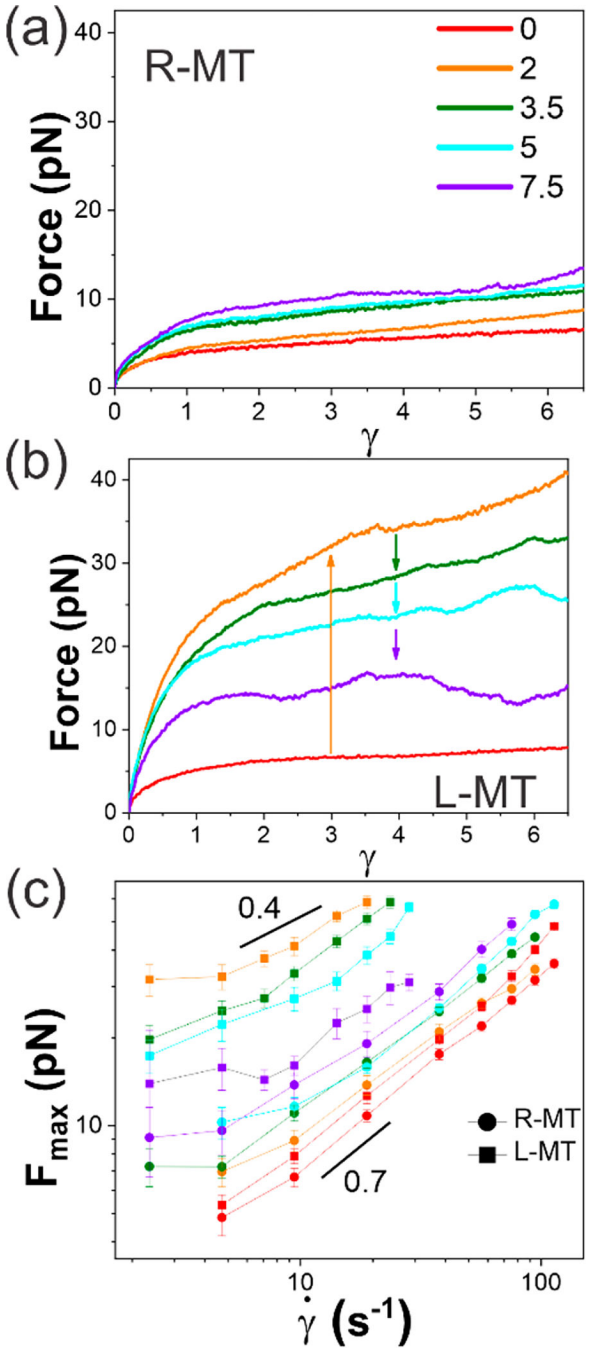

Figure 3.

The nonlinear force response of DNA-MT composites exhibits a complex dependence on DNA topology, tubulin concentration, and strain rate. (a, b) Measured force in response to strain of rate $\dot{\gamma} = 9.4\ s^{-1}$ for composites with ring (a) or linear (b) DNA and varying tubulin concentrations listed in μM in the legend. Arrows point in the direction of increasing tubulin concentration to guide the eye. Similar to the linear regime, L-MT composites exhibit greater force response than R-MT composites and a strong nonmonotonic dependence on tubulin concentration that is lacking in R-MT composites. (c) Maximum force reached

during strain F_{max} vs strain rate $\dot{\gamma}$ for R-MT (circles) and L-MT (squares) composites with varying tubulin concentrations shown in the legend in (a). Black lines represent power-law scaling with exponents shown. In general, composites with higher force responses have weaker dependence on strain rate, signifying a more elastic response. Error bars, some of which are smaller than the symbol size, represent the standard error from 15 trials. We note that scaling exponents determined from the data should be considered approximate due to the limited range evaluated for some cases.

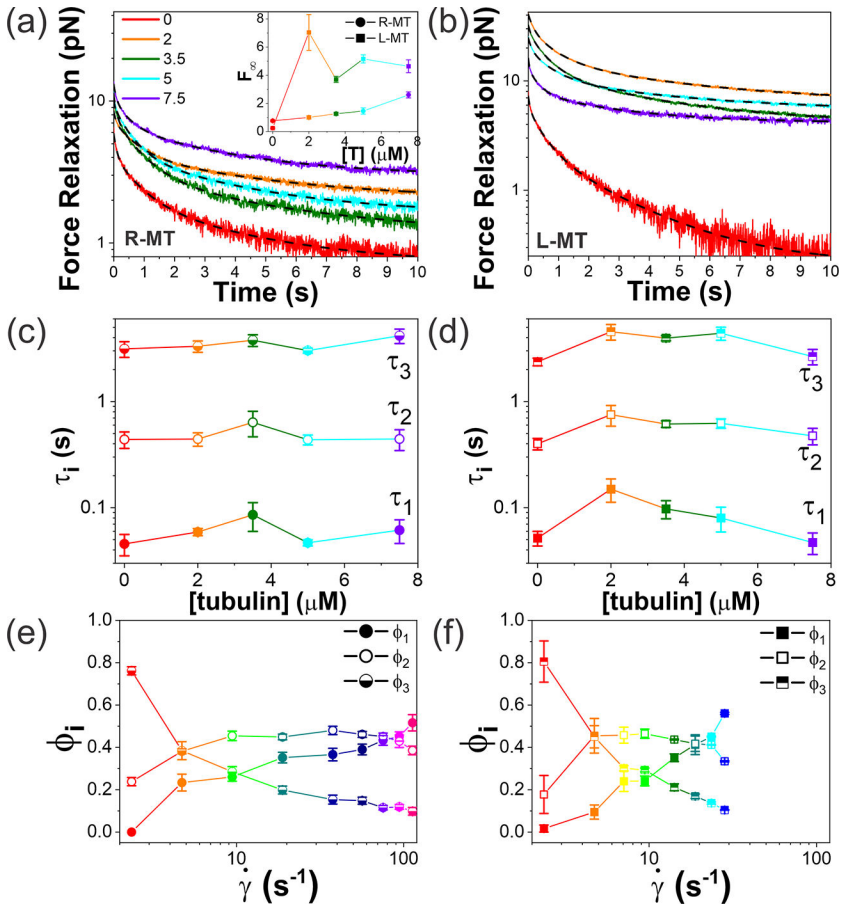

Figure 4.

DNA-MT composites exhibit multimode relaxation and sustained memory following nonlinear straining. (a, b) Force relaxation of composites with ring (R-MT, a) or linear (L-MT, b) DNA and varying tubulin concentrations (shown in μM in legend) following a $\dot{\gamma} = 9.4$ s^{-1} strain. Each relaxation curve is fit to a sum of three exponential decays and a residual: $F(t) = F_\infty + C_1e^{-t/\tau_1} + C_2e^{-t/\tau_2} + C_3e^{-t/\tau_3}$. Sample fits (all of which have adjusted R-squared values of ≥0.99) are shown as black dashed lines. Three time constants are necessary and sufficient for best possible fits. (Inset) DNA-MT composites exhibit sustained elasticity as shown by the nonzero force maintained at the end of the relaxation phase F_∞, shown averaged over all $\dot{\gamma}$ as a function of tubulin concentration. (c, d) Time constants τ_1, τ_2, and $\tau 3$, determined from fits and averaged over all $\dot{\gamma}$, as a function of tubulin concentration for R-MT (circles, c) and L-MT (squares, d) composites. (e, f) Corresponding fractional amplitudes ϕ_1 [$=C_1/(C_1 + C_2 + C3)$], ϕ_2, and ϕ_3 determined from fits, averaged over all tubulin concentrations and plotted versus $\dot{\gamma}$ for R-MT (circles, e) and L-MT (squares, f) composites. Fractional amplitudes for both R-MT (circles) and L-MT (squares) composites show that fast relaxation modes (τ_1 and τ_2) become increasingly dominant at high strain rates, whereas the slowest mode ($\tau 3$) dominates at low strain rates. Fractional amplitudes for $\dot{\gamma} > 30$ s^{-1} are not available for L-MT composites, as the composite resistive force exceeds the trapping force. Error bars for all panels, some of which are smaller than the symbol size, represent the standard error from 15 trials.

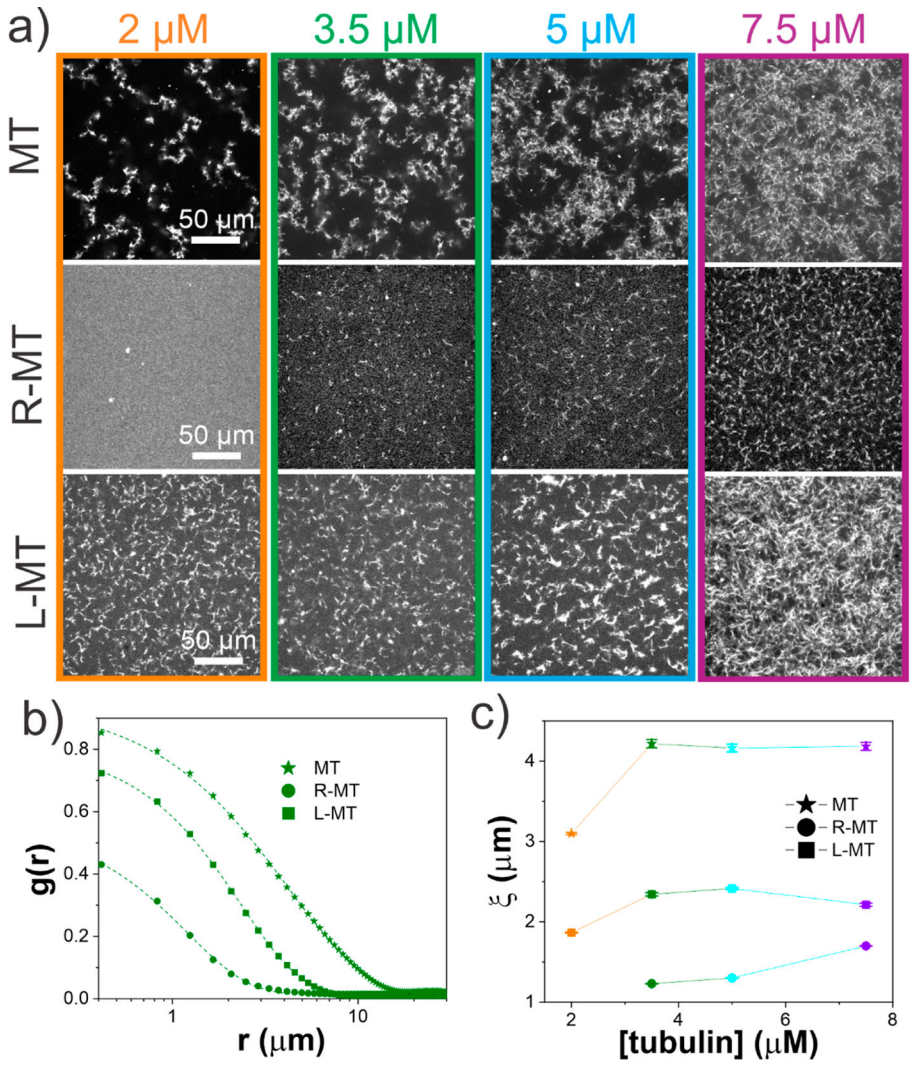

Figure 5.

DNA end-closure dictates the degree of polymerization and flocculation of microtubules in DNA-MT composites. (a) Confocal micrographs of microtubules polymerized from rhodamine-labeled tubulin dimers of varying concentrations (listed above each row and color-coded as in (c)) in buffer (MT, top), ring DNA solutions (R-MT, middle), and linear DNA solutions (L-MT, bottom). (b) Average spatial image autocorrelation curves $g(r)$ computed from confocal images for [tubulin] = 3.5 μM (see Figure S2 for a complete set of autocorrelation curves). (c) Structural correlation lengths ξ determined from fits of the autocorrelation curves to $g(r) \propto e^{r/\xi}$ for all cases shown in (a). Error bars, some of which are smaller than the symbol size, are determined from fits to corresponding $g(r)$ curves.

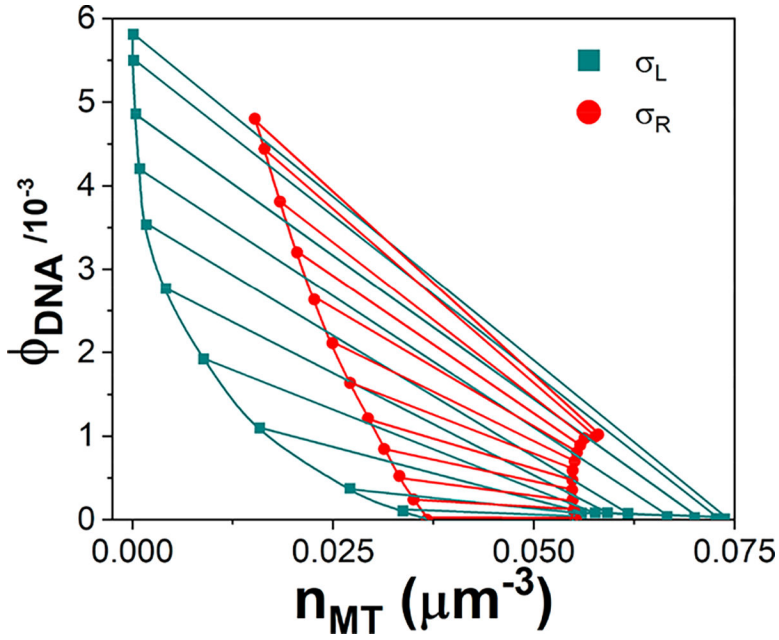

Figure 6.

Depletion-induced isotropic-to-nematic transition describes the nonmonotonic mechanical response and flocculation in DNA-MT composites. Phase diagram showing results using SPT[72] for a composite of rod-like particles (MTs) and flexible polymer coils (DNA) for varying DNA volume fraction ϕ_{DNA} and MT number concentration n_{MT} (see the SI for a description of the theory and calculations). The points mark the binodal lines separating the isotropic (left) and nematic (right) phases for the microtubules in the presence of ring (σ_R, red) or linear s(σ_l, dark cyan) DNA. The lines connecting the binodals are the corresponding tie lines. Note the only difference taken into account between ring and linear DNA is their different coil size σ. The coexistence regions between the binodals, indicate the region in which isotropic and nematic MT phases coexist, which manifests as MT flocculation in experiments. Note that the coexistence region is significantly smaller for ring DNA and shifted toward higher n_{MT} values, as seen in experiments (Figure 5).